A Numerical Simulation of the Landfall of Tropical Cyclones

ROBERT E. TULEYA AND YOSHIO KURIHARA

Geophysical Fluid Dynamics Laboratory/NOAA, Princeton University, Princeton, N. J. 08540

(Manuscript received 6 June 1977, in final form 20 September 1977)

ABSTRACT

A GFDL tropical cyclone model was applied to simulate storm landfall. The numerical model is a three-dimensional, primitive equation model and has 11 vertical levels with four in the planetary boundary layer. The horizontal grid spacing is variable with finest resolution being 20 km near the center. This model was used successfully in the past to investigate the development of tropical cyclones over the ocean.

In the present experiments, a simple situation is assumed where a mature tropical cyclone drifts onto flat land. In such a case, the landfall can be simulated by changing the position of the coastline in the computational domain rather than by moving the storm. As the coastline moves with a specified speed, the surface boundary conditions are altered at the shore from those for the ocean to those for the land by increasing the surface roughness length and also by suppressing the evaporation.

Despite the simplicity and idealization of the experiments, the cyclone's filling rates are quite reasonable and a decay sequence is obtained. Notable asymmetries in the wind, moisture and precipitation fields exist relative to the coastline at the time of landfall. Roughness-induced, quasi-steady convergence and divergence zones are observed where onshore and offshore winds encounter the coastline. Spiral bands propagate and exist over the land area. A comparison of the energy and angular momentum budgets between ocean and land surface boundary conditions indicates a simultaneous broadening and weakening of the storm system in the decay process. The latent energy release through condensational processes is initially augmented over land by greater moisture convergence in the planetary boundary layer which counteracts the lack of evaporation from the land surface.

Supplementary experiments indicate that the suppression of evaporation is the most important factor in the decay of a storm upon landfall. When the evaporation is suppressed, the storm eventually weakens whether the surface roughness is increased or not. An increased surface roughness, which causes increased inflow in the boundary layer, has little immediate negative impact on the storm intensity. Indeed, if the supply of latent energy is sufficient, a storm can deepen when encountering an increase in surface roughness. The decay rate in a later period well after landfall is influenced by the rate with which the water vapor of the storm system is depleted in the earlier period immediately after landfall.

1. Introduction

Both axisymmetric and three-dimensional numerical models of tropical cyclones have been successfully integrated and extensively analyzed at the Geophysical Fluid Dynamics Laboratory/NOAA. The results of a three-dimensional experiment were published by Kurihara and Tuleya (1974) and Tuleya and Kurihara (1975). In this study, this basic model is used to simulate an idealized landfall of a tropical cyclone. The purpose of this paper is to describe the structural changes and to clarify the decay processes of a mature tropical cyclone through the analysis of the results of several experiments. The relative influence of the depletion of evaporation and of increased surface roughness in the maintenance and decay of a tropical cyclone upon landfall are discussed in particular. Landfall may be defined, specifically, as the instant of time when the center of a tropical cyclone encounters the coastline. More generally, landfall may be considered to be the process of the entire storm system moving over land. In this study the first definition is used primarily, although the second definition is used to describe the event in general.

Some modeling studies have investigated the sensitivity of tropical cyclones to surface boundary conditions. Ooyama (1969) noted that the simulated mature hurricane in his model cannot maintain hurricane intensity more than 15 h if the supply of thermodynamic energy from the underlying surface is cut off. He also discussed the effect of surface friction change on the evolution of a tropical vortex. Rosenthal (1971) studied the effect of changing drag coefficients for momentum and sensible and latent heat at different stages of a model cyclone's development. The apparent dual role of increased surface friction, i.e., the direct effect of surface drag and the effect of increased Ekman pumping were mentioned in these investigations. The models in these studies were axisymmetric, used a single layer to represent the planetary boundary layer and featured abrupt, instantaneous changes in the surface boundary conditions. In the present study, however, a three-dimensional model is utilized, in which changes in surface boundary conditions can be elaborated to simulate a storm landfall more realistically and the development of asymmetries in the wind, pressure and precipitation fields may be anticipated.

Also, the vertical resolution of the present model enables one to explicitly study changes in the boundary layer structure at landfall.

A considerable number of observational studies of tropical cyclones at landfall were made with various objectives in mind. Miller (1964) analyzed the surface energy fluxes, surface dissipation and the related structural and thermodynamic changes of Donna (1960) upon landfall, Koteswaram (1963) investigated precipitation anomalies of several Indian cyclones and Novlan and Gray (1974) summarized the climatology of hurricane landfall and the spatial relationship of the storm center to the position of spawned tornadoes. The comparison between the present results and these observations will be discussed as well as the limitations of the present model's experimental framework.

In Section 2 a brief review of the model is given followed by the design and strategy of landfall simulation. The time integration of the basic landfall experiment is discussed in Section 3 including a detailed analysis of the three-dimensional structural changes occurring at landfall. Section 4 contains a concise, vertically integrated analysis of the budgets of kinetic, total potential and latent energy as well as a budget analysis of relative angular momentum. Results of additional experiments to analyze the relative role of moisture depletion and increased roughness in the decay sequence are given in Section 5. These additional experiments help to define a time sequence of the decay mechanisms responsible for storm filling when encountering land. Finally, the results are summarized in Section 6.

2. Experimental design

a. Review of model

The basic tropical cyclone model is that developed by Kurihara and Tuleya (1974). It has 11 levels with four in the planetary boundary layer. The horizontal resolution is variable with 20 km grid spacing near the center. The 4000 km square domain is closed and the box method is utilized in the finite-difference formulation of the primitive equations. An Euler backward scheme is applied in the time integration (Matsuno, 1966; Kurihara, 1965). The cumulus parameterization scheme used is one developed by Kurihara (1973). A Monin-Obukov type framework is used to estimate the surface fluxes at the lower boundary. A stability-dependent mixing length formulation is used for diffusion of heat, moisture and momentum above the constant flux layer. In the present experiments, the surface boundary conditions were altered from those of the basic model to account for a storm system encountering land.

The numerical integration carried out previously with the above mentioned basic model (Kurihara and Tuleya, 1974) will be called hereafter the control experiment. The tropical cyclone was successfully simulated in the control experiment, in which the entire lower boundary was the ocean with the surface temperature fixed at 302 K. A storm developed from an initially specified weak vortex and at hour 89 of the model integration, the central pressure was 962 mb with maximum surface winds greater than 45 m s^{-1}. An upper level warm core of approximately 10 K difference between the center and the outer region of the storm was observed at this time. Moisture, which is an energy source for a tropical cyclone, was supplied through the sea surface boundary and advected spirally inward in the shallow, low-level boundary layer. Spiral bands developed and moved radially outward.

b. Strategy of experiments

In order to avoid possible complications associated with an attempt to move a tropical cyclone by a steering current and to utilize a tested numerical framework, the simulations of hurricane landfall were performed under simple conditions and approximations. In lieu of an actual steering current moving the model vortex, the position of land-sea interface was shifted through the grid domain at a constant speed with separate surface boundary conditions specified over the land and ocean areas. In these experiments the surface drag caused by the relative movement between the steering current of the storm and the surface boundary was not taken into account. This is probably one of the most elementary designs of a landfall experiment. Obviously, this precluded studying any interactions between the storm and the steering current systems. Such interactions may be quite important in some cases of actual tropical cyclone decay. For instance, as a cyclone progresses toward mid-latitudes, baroclinic features of the basic field become prevalent and the tropical cyclone may take on extra-tropical characteristics. Another factor not included in the present experiments is the incursions of cold and dry air from continental areas. In the present model framework, only modification of the storm system is possible through changes in surface boundary fluxes.

The initial state of the model in the landfall experiments was provided from the field at hour 89 of the control experiment. The land-sea interface was assumed at this time at approximately 800 km from the storm center and was shifted at a constant speed of 10 m s^{-1} toward and through the storm during the integration.

When the coastline moved through specific grid boxes, the surface boundary conditions were appropriately changed from those of sea to those of land. In the Monin-Obukhov framework the downward flux of momentum τ the sensible heat flux H and the water vapor flux E at the surface are computed from the

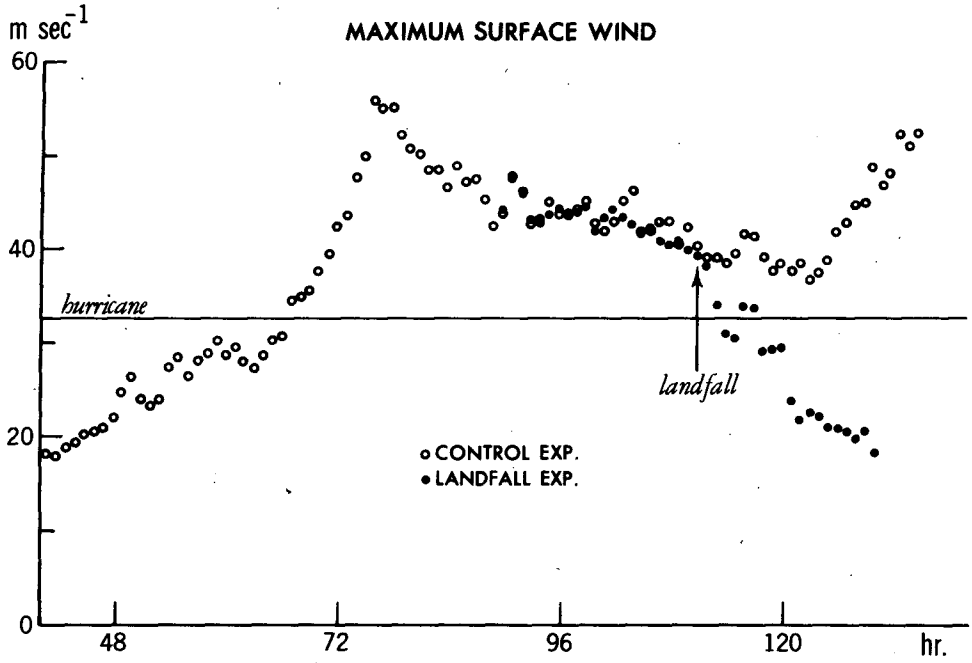

FIG. 1. Time variation of maximum surface wind. Basic landfall experiment was initiated from control experiment at 89 h.

following set of formulas:

$$\left.\begin{aligned} \tau &= \rho \mathbf{V}_*^2 \frac{\mathbf{V}(h)}{|\mathbf{V}(h)|} \\ H &= \rho C_p |\mathbf{V}_*| \theta_* \\ E &= \rho |\mathbf{V}_*| r_* \end{aligned}\right\}, \tag{2.1}$$

where ρ is the density of air, C_p the specific heat at constant pressure, $\mathbf{V}_*$ the friction velocity, θ_* the frictional potential temperature, r_* the frictional mixing ratio and $\mathbf{V}(h)$ the vector wind at height h. The top of the constant flux layer h is assumed to extend up to the lowest model level ($\sim$68 m). The frictional values ($\mathbf{V}_*$, θ_*, r_*) are obtained iteratively when $\mathbf{V}(h)$, $\theta(h)$ and $r(h)$ are given, $\theta(0)$ and $r(0)$ are specified and the formula for the surface roughness length z_0 is chosen (Kurihara and Tuleya 1974, p. 897). The values $\theta(0)$ and $r(0)$ may be changed from sea to land conditions. The length z_0 is calculated using Charnock's relation

$$(z_0)_\vartheta = 0.032 \frac{|\mathbf{V}_*|^2}{g} \tag{2.2}$$

for ocean conditions. For land surface boundary conditions $(z_0)_l$ is specified. The suffixes ϑ and l will be used to denote ocean and land, respectively.

For the present experiments, $\theta(0)$ was fixed at 302 K over both land and sea. The quantity $r(0)$ can be formulated as

$$r(0) = \begin{cases} r_{\mathrm{SAT}} \cdot w & \text{for land} \\ r_{\mathrm{SAT}} & \text{for ocean} \end{cases} \tag{2.3}$$

where r_{SAT} is the saturation mixing ratio at the surface. In these experiments w was set to either 0.0 or 1.0 and the surface evaporation was never allowed to go below zero. The roughness length over land was either given a value of 25 cm or approximated by the formula (2.2). Given these boundary conditions for either land or sea, the fluxes could be evaluated using (2.1). If a grid box was part land and part ocean, the fluxes were then weighed in proportion to the relative area in the grid box.

c. *Basic experiment*

For extensive analysis, one basic landfall experiment was integrated. The values for the land conditions were: $(z_0)_l = 25$ cm and $E_l = 0$ (zero evaporation). The formulation of the surface fluxes over the ocean was identical to those of the control experiment. The value of $(z_0)_l$, 25 cm, was selected to be relatively high to exaggerate the land-sea roughness difference, but still less than a typical value for urban or forest area (Sellers, 1967). As a crude approximation, the evaporation was set to zero over the land area since, compared to the sea surface temperature, the actual land surface temperature may be expected to be cold and the land area may not be wet everywhere. This reduces the potential evaporation from the surface. Observational evidence of Miller (1964) indicates the evaporation to be negligible over land when a hurricane encounters a coastline. The results of the basic experiment are discussed and analyzed in Sections 3 and 4.

d. Supplementary experiments

To clarify the mechanism of storm decay by isolating the effects of surface roughness and the effects of evaporation depletion, respectively, two supplementary experiments were integrated. One experiment was identical to the basic landfall experiment except that the land surface was assumed to be smooth. Charnock's relationship was used to estimate the land's roughness length as well as the ocean's roughness length. The evaporation was again totally depleted over land. The second supplementary experiment simulated a cyclone undergoing an increase in surface roughness without any depletion of evaporation. Over assumed wet land, the roughness length was increased to 25 cm and the evaporation was not suppressed. As in the basic experiment, the two supplementary landfall experiments used the control model's conditions at hour 89 as initial conditions, the coastline was placed approximately 800 km from the storm center and the experiments were integrated to hour 130 while the coastline was shifted with the speed 10 m s^{-1}. The results of the supplementary experiments are discussed in Section 5.

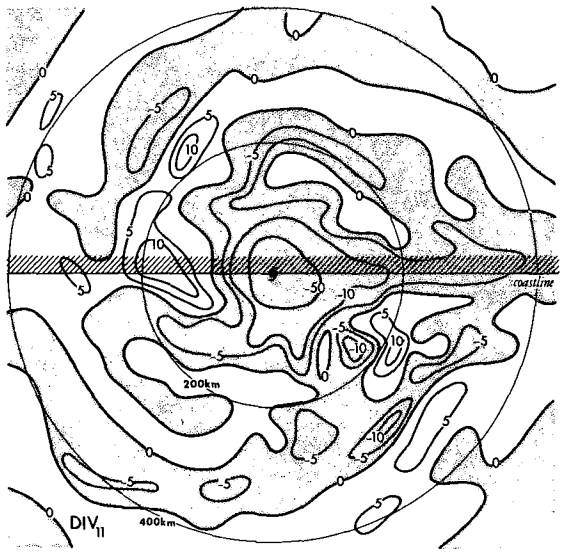

FIG. 3. Distribution of divergence of wind at level 11 (10^{-5} s^{-1}) at hour 111 for basic landfall experiment. Areas of convergence are shaded.

3. Results of the basic landfall experiment

a. Wind field

The maximum surface winds of the basic landfall experiment can be compared with those of the control experiment in Fig. 1. For the first 20 h of integration of the landfall experiment there is little difference in the maximum wind speeds until landfall. The decrease in surface winds after landfall is due to both the direct frictional effect of an increase in surface roughness and the overall decay of the storm system. Three hours after landfall the surface winds decrease below hurricane force and remain below hurricane force after 6 h from landfall. The maximum surface winds fall below 20 m s^{-1} in about 12 h after landfall as the tropical cyclone continues to decay and dissipate over the land area.

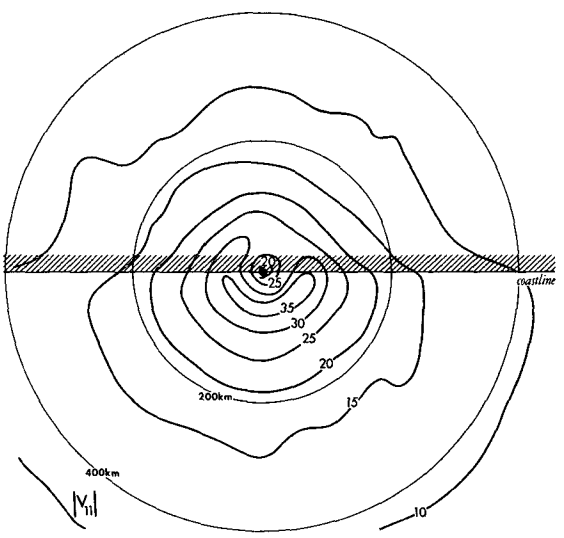

FIG. 2. Distribution of surface wind speed, level 11 for the basic landfall experiment at the time of landfall, hour 111. Units are in m s^{-1}.

At the time of landfall, the wind field of the basic experiment was extensively analyzed. One can immediately see the impact of the rough land on the surface winds as the maximum winds are confined to the ocean and the area of gales is considerably reduced over the land compared to that over the ocean (Fig. 2). This reduction of wind speed is confined only to the boundary layer and is a direct result of the increased loss of momentum over the rough land relative to the smooth ocean. The reduction of wind speed is due mainly to the reduction of the tangential component of the flow. Except for the lowest level the radial component significantly increases from ocean to land. This point will be discussed further in the latter part of this subsection.

Fig. 3 shows the distribution of the divergence field at level 11 at landfall. Spiral bands observed to exist by Kurihara and Tuleya (1974) in the control experiment still exist over land as well as ocean. The bands propagate outward from the center, and there is no noticeable difference in the structure between the bands over the ocean and over the land. Of course, as the storm weakens later, these bands also become less intense. Beside the spiral bands, Fig. 3 also shows coastline bands of convergence and divergence with approximately the same amplitude as the spiral bands. The bands play a role in the boundary layer distribution of moisture and subsequent precipitation patterns. Notice that in the outer regions of the coastal convergence zone, the order of magnitude of the conver-

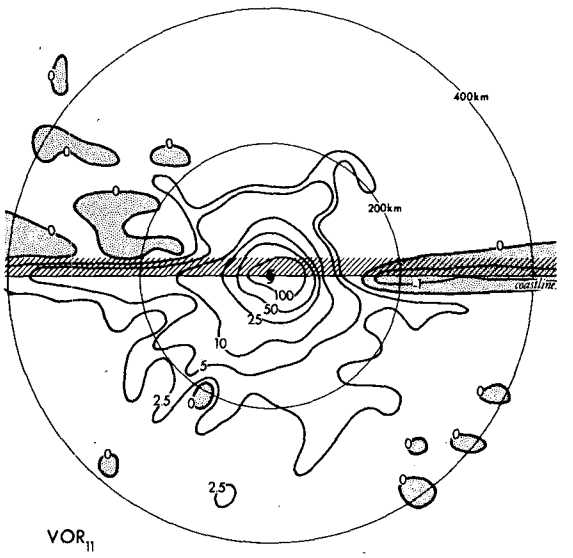

FIG. 4. Distribution of vorticity of wind at level 11 (10^{-5} s^{-1}) at hour 111 for basic landfall experiment. Areas of negative relative vorticity are shaded.

gence is typically 10^{-5} s^{-1} where winds blow ashore at $\sim$15 m s^{-1}. These bands have relatively little precipitation associated with them. The coastline bands exist throughout the integration but are most pronounced when the maximum winds are near the coastline, i.e., at landfall.

Another low-level feature of interest at landfall is the relative vorticity field at the surface (Fig. 4). In addition to the vorticity maximum near the center, there is a band of large positive vorticity where winds blow offshore and a band of negative relative vorticity where winds blow onshore. In cylindrical coordinates, the relative vorticity is defined by $\partial(rv_\theta)/r\partial r - \partial v_r/r\partial\theta$, where r is the radius, v_θ is the azimuthal component of wind and v_r the radial component, respectively. A quantitative analysis indicates that the second term in the above definition of vorticity causes the shoreline vorticity anomalies. Accordingly, the band of negative vorticity can be attributable to the decrease in the surface inflow across the shoreline. Such a feature is confined only to a shallow layer at the surface. Like the divergence bands, the vorticity bands exist at the shoreline throughout the integration.

A significant change in the wind structure of the boundary layer occurs when the tropical cyclone encounters land. Fig. 5 portrays the boundary layer profiles of the radial and tangential components of the wind at 110 km radius over land (4–8 h after landfall)

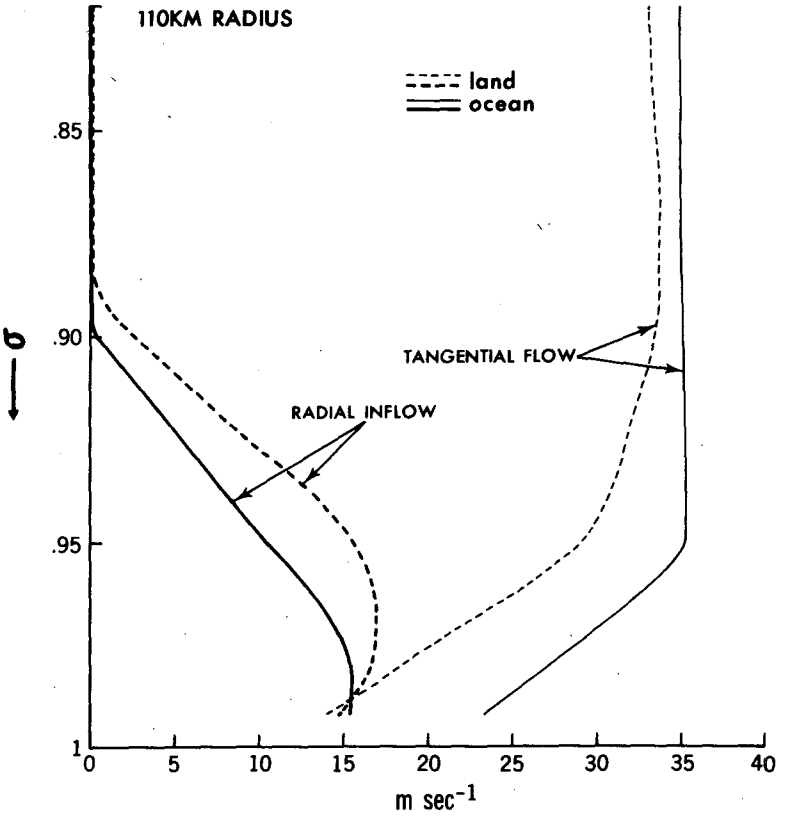

FIG. 5. Vertical profiles of tangential and radial wind in the surface boundary layer over ocean (hours 103:15–107:00) and over land (hours 115:00–118:45). Profiles are from the basic landfall experiment at a radius of 110 km from the storm center.

and also over sea (4–8 h before landfall). It is seen that the tangential wind component is reduced over land, while the radial component is dramatically increased over land between a height of ~100 m and ~900 m. At the bottom level only, the radial wind is less over land than over ocean. The inflow layer becomes somewhat thicker. Because of the decrease in tangential component of the wind, the kinetic energy in the boundary layer is significantly reduced over land. Boundary layer flow in a circular vortex was discussed by Syono (1949), Yanai (1964) and Eliassen (1971). The change in the boundary layer wind after landfall in the present numerical experiment can be deduced from these studies. The inflow increase contributes to increases in moisture convergence and kinetic energy generation. These effects tend to counteract the obvious increase in dissipation of kinetic energy at the surface and decrease in evaporation over land. Accordingly, a tropical cyclone may maintain its intensity at least for a while after landfall or even deepen under certain circumstances. As the evaporation is suppressed over land, the environment of a tropical cyclone becomes less humid and the storm ultimately decays. Rosenthal (1971) discussed the possible dual role of an increase in drag coefficients in some model experiments.

b. Surface pressure and storm track

The track of the storm can be seen in Fig. 6. The center of the storm, which is defined as the position of the surface pressure minimum, is marked at 5 h intervals by a hurricane symbol and the central surface pressure is indicated at these times. Landfall was

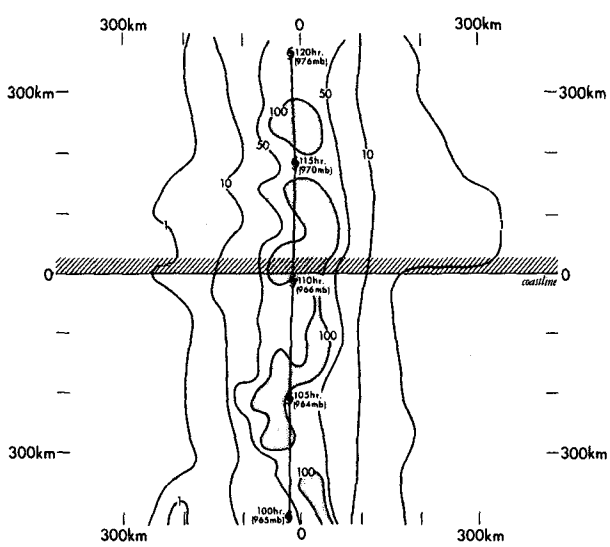

FIG. 6. Tropical cyclone path for basic landfall experiment. Position of center plotted at 5 h intervals by use of hurricane symbol. Central surface pressure indicated at specified times. Total rainfall (mm) for the entire basic experiment is also contoured.

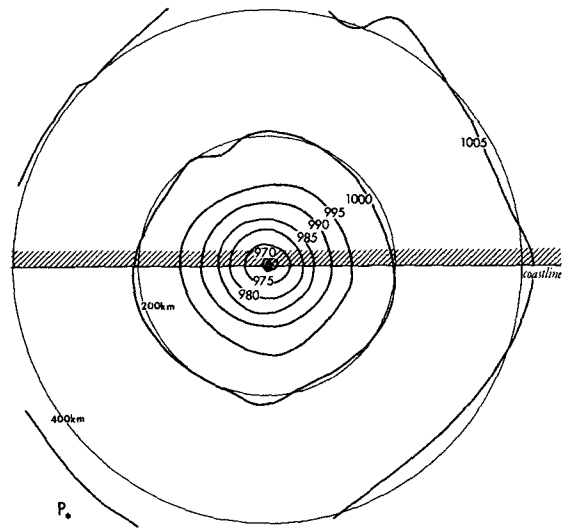

FIG. 7. Distribution of surface pressure (mb) at hour 111 for the basic landfall experiment.

reached at hour 111. Until then there was little increase of the central surface pressure. The direction and speed did not show any obvious anomalies at the time of landfall. As the tropical cyclone drifted over land, there was no tendency for the storm center to remain over the ocean. As shown in Fig. 7, the surface pressure distribution is nearly circular with pressures below 1000 mb being confined to the inner 200 km of the storm. The surface pressure pattern remained circularly symmetric throughout the integration period. The central surface pressure rose from 966 mb at hour 110 to 989 mb at hour 130. The most rapid filling was not at the time of landfall, but about 5 h after the storm center encountered land. At this time, the central surface pressure filled at a rate of 3 mb for a 1 h period. The surface pressure did not increase uniformly throughout the storm but rose most rapidly at the center. At radii greater than 150 km, the surface pressure increased less than 1 mb from landfall to hour 125. This can be seen by the solid curves in Fig. 8 which show the radial distribution of surface pressure at three time periods for the basic landfall experiment. These results are similar to the observations of Miller (1964) and Syono *et al.* (1951) which indicate that initial storm filling is confined to a rather small area near the storm center.

c. Temperature field

The surface pressure distribution of the tropical cyclone is approximately a reflection of the temperature distribution observed aloft. The dashed lines in Fig. 8 depict the radial distribution of temperature at $\sigma=0.215$ of the model (scale shown at the right ordinate). The warm core is most intense at this height. Notice that the temperature near the center decreases slowly from hour 105 to hour 115. Four hours after landfall the

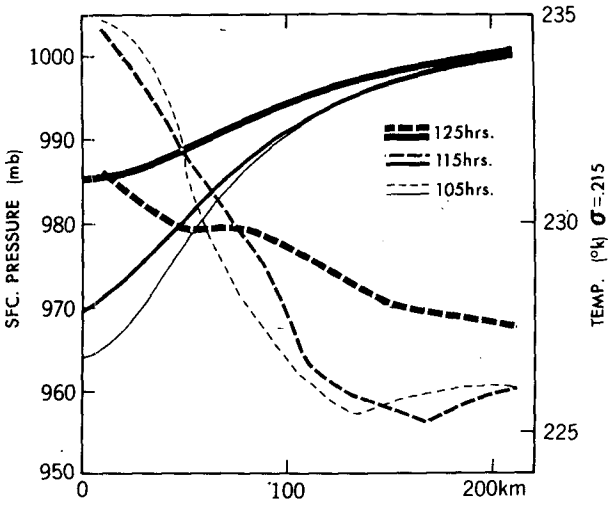

FIG. 8. Radial distributions of surface pressure (mb, left scale) and upper level temperature (K, right scale) for basic landfall experiment. The temperature plotted is that for the third level, $\sigma=0.215$, or ~11 242 m height. Distributions at three times, representing before, during and after landfall respectively, are shown.

horizontal gradient of temperature is reduced because of a slight temperature decrease near the center and a slight increase beyond 50 km. A more dramatic decrease of three degrees in the warm-core temperature occurs from hour 115 to hour 125. A general warming beyond 90 km in this period reduces the 0–200 km temperature gradient from 9 to 4 K. The reduction in the temperature gradient near the storm center, together with an increase in the temperature gradient beyond 100 km, indicates an overall broadening of the storm as its maximum intensity decreases. The warm core is maintained by a delicate balance among the cooling process of adiabatic ascent, the heating process of condensation, and the effect of large-scale advection. Initially at landfall in the basic experiment, the increased radial-vertical circulation caused by increased Ekman pumping has only a minor effect on the upper level warm core. This is because the increased dynamic cooling is almost compensated by the increase in latent heat release.

d. Moisture and precipitation patterns

The moisture field is dramatically altered when the storm encounters land because of the total elimination of evaporation from the land surface. This is apparent in Fig. 9 at the time of landfall. A region of relative humidity below 80% occurs to the left of the storm. The surface air becomes progressively drier as it blows cyclonically around the hurricane vortex until it reaches its driest value at the coast where it acquires moisture again through evaporation. The dramatic front in the moisture field to the left of the storm is further enhanced by drier air brought down to the surface layer in the coastline divergence zone. This moisture decrease obviously reduces the surface equivalent potential temperature and causes a decrease in conditional instability as this dry air is advected radially into the very heart of the storm core.

The rainfall distribution associated with the basic experiment indicates an intense narrow swath centered along the path of the tropical cyclone. This can be seen in Fig. 6. Rainfall totals of over 100 mm are common both over land and over ocean, and there is no tendency for a decrease in rainfall for the first 300 km inland. In fact, some tendency for an increase in rainfall exists to the right of the storm track where winds blow onshore. During and after landfall, the position of maximum precipitation is biased toward the upper right quadrant of the storm. Fig. 10 shows the point distribution of maximum precipitation, plotted every 15 min, before landfall (hours 103:00–108:45) and during landfall (hours 109:00–114:45). Before landfall, as one might expect, the pattern is more or less random with approximately the same number of points located in each quadrant relative to the moving storm. Upon landfall a significantly large number of points (79%) fall in the quadrant to the upper right. In this quadrant, excess precipitation is caused by ample moisture advected from the ocean and enhanced boundary layer convergence. Koteswaram (1963) summarized observations of rainfall from Indian cyclones indicating a bias to the right of the storm path. It is interesting to note that Novlan and Gray (1974) discussed a bias in tornado activity in the same upper right quadrant of the storm. This observed bias, if significant, is consistent with the model's result provided that there exists a positive correlation between heavy precipitation in the model and tornadic activity.

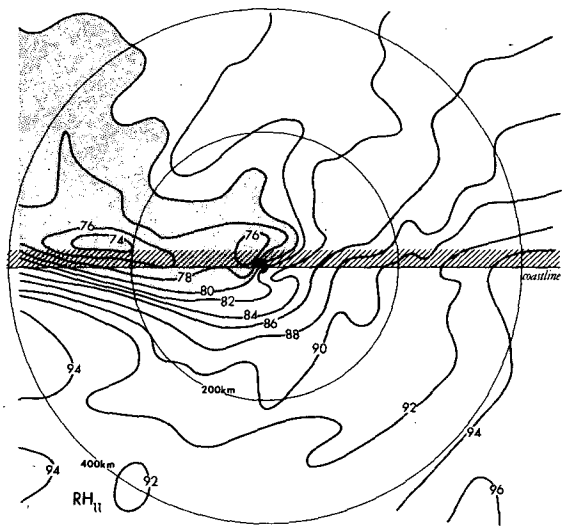

FIG. 9. Distribution of relative humidity at level 11 (%) at hour 111 for basic landfall experiment. Values less than 80% are shaded.

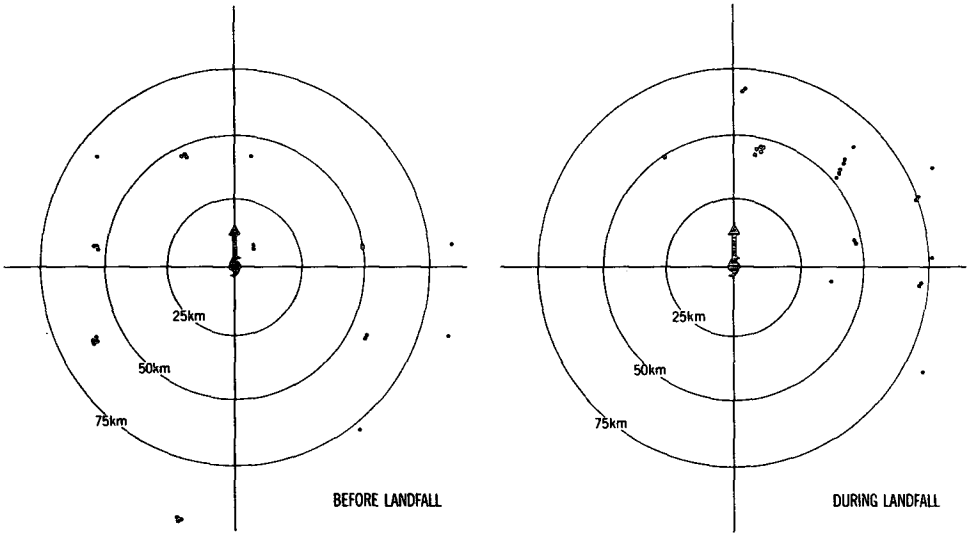

FIG. 10. Distribution of points of maximum precipitation before (hours 103:00–108:45) and during (hours 109:00–114:45) landfall in the basic landfall experiment. Points shown are plotted every 15 minutes relative to the moving storm center.

A time-averaged field (hour 97:15–126:45) of ω, dp/dt, at level 9 is shown in Fig. 11. This level is approximately at the top of the planetary boundary layer. Zones of upward and downward motion occur where onshore and offshore winds encounter the coast. Also notice the increased vertical velocity over the land along the storm's path. The increase in upward motion in these areas tends to augment the rainfall. Actually, the precipitation rate over the entire domain is greater in the basic landfall experiment than in the control experiment for a 7 h period during and after landfall and becomes smaller relative to the control experiment only gradually with time. This feature is shown in the upper part of Fig. 12. The precipitation intensity is a measure of the rate of latent energy release. The lower part of Fig. 12 shows the deviations of both the dissipation and generation of kinetic energy from the control experiment. Both quantities exhibit fluctuations similar to that of the latent energy release. They exceed the values of the control experiment immediately after landfall and become relatively small as the storm later weakens. A large negative deviation of the generation after hour 120 is consistent with the decrease in the rainfall rate.

4. Energy and angular momentum analysis

In this section, characteristic changes of the energy and angular momentum budgets due to landfall are investigated. For this purpose the budgets were computed and compared for three time periods of the basic landfall experiment: before landfall (hours 103:15–107:00), at landfall (hours 109:15–113:00) and after landfall (hours 115:00–118:45). Most of the results shown and discussed in this section are for the periods before and after landfall. The procedures taken for this analysis are those utilized by Tuleya and Kurihara (1975) except that the total energy was not separated into mean and eddy components. The energy and angular budget terms were computed along azimuthal rings surrounding the location of the central surface pressure.

a. Kinetic energy budget

For the entire domain, the generation of total kinetic energy rises abruptly at landfall and then irregularly decreases to progressively lower values relative to the

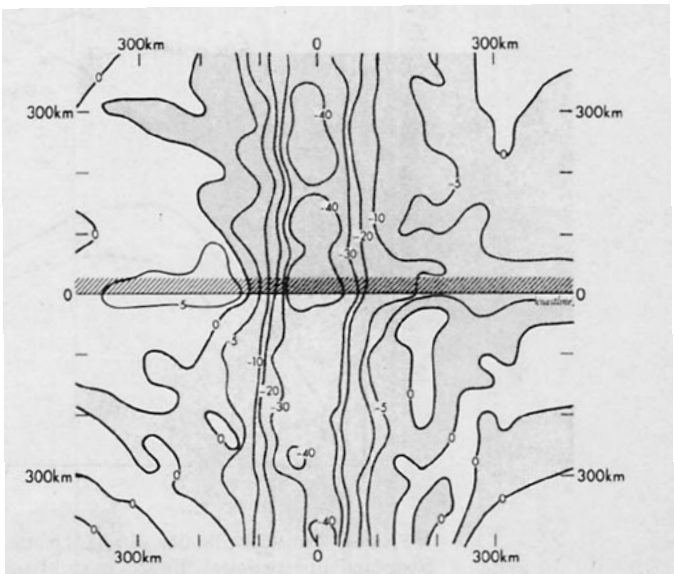

FIG. 11. Time average (hour 97:15–126:45) of spatial distribution of ω for the ninth model level for the basic landfall experiment. Units are in 10^{-4} mb s^{-1}. Areas of negative ω are shaded.

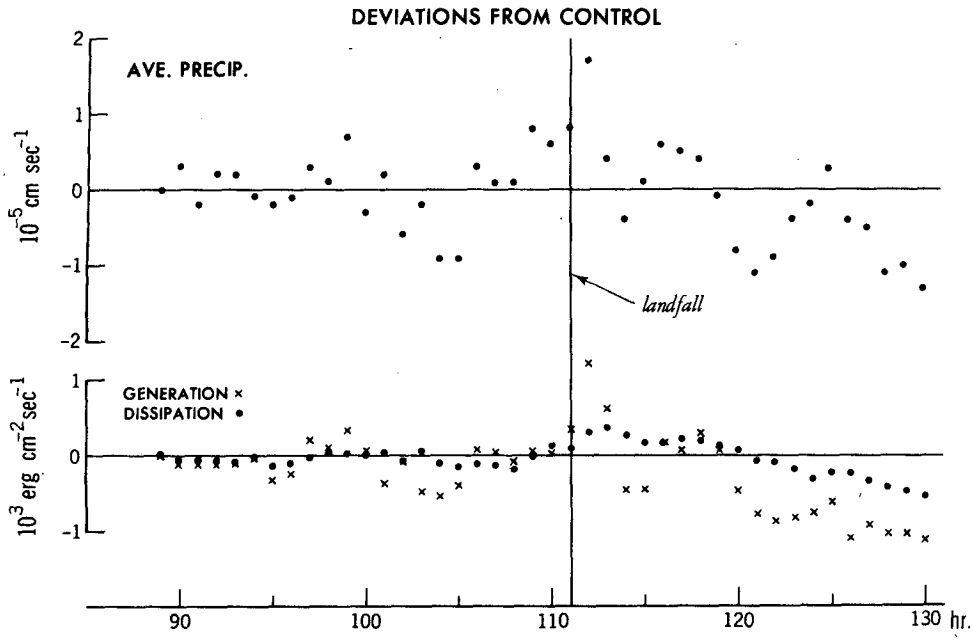

FIG. 12. Time variation of comparison of average precipitation, generation and dissipation between control experiment and basic landfall experiment. Figures given are deviations of the basic landfall experiment from the control experiment and apply to the entire grid domain.

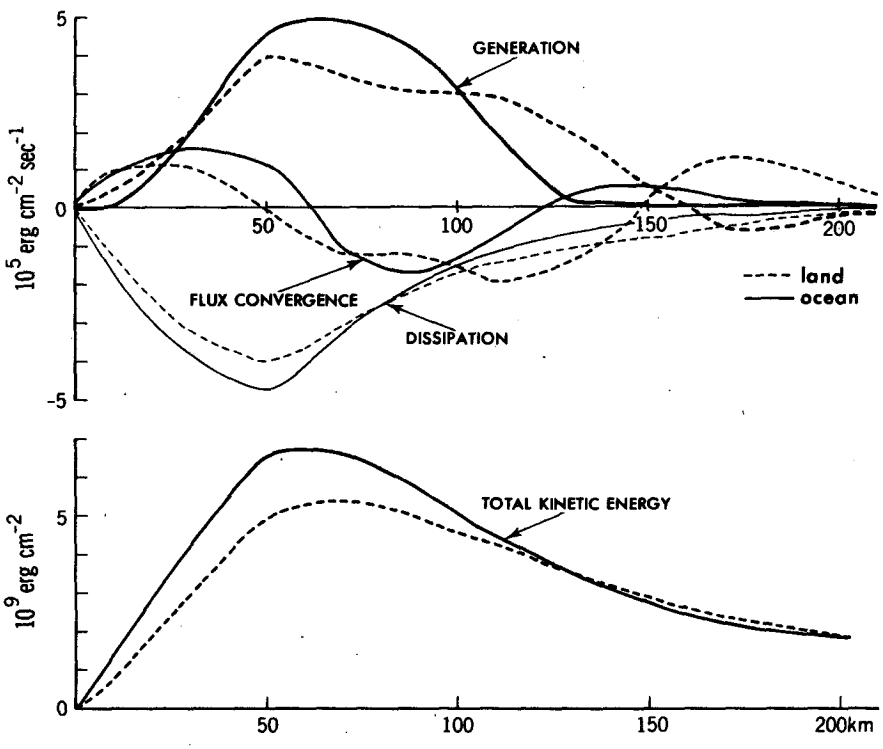

FIG. 13. Radial distribution of total kinetic energy and total kinetic energy budget for the basic landfall experiment. Budget quantities are shown for period over ocean (hours 103:15–107:00) and for period over land (hours 115:00–118:45). Changes due to generation from potential energy (thick lines), flux conversion (medium line) and dissipation (thin lines) are indicated for both periods. Budget terms are vertically integrated, circularly averaged.

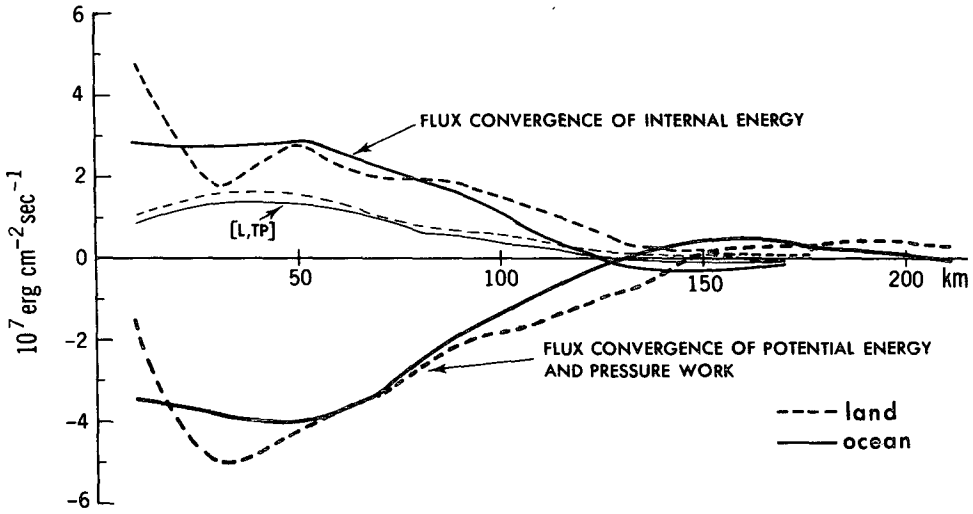

FIG. 14. Radial distribution of budget of total potential energy for the basic landfall experiment. Budget quantities are shown for the period over ocean (hours 103:15–107:00) and for the period over land (hours 115:00–118:45). Changes due to flux convergence of potential energy and pressure work (thick lines), flux convergence of internal energy (medium lines), and conversion of latent heat (thin lines) are indicated for both periods. Budget terms are vertically integrated, circularly averaged.

control experiment. The increase at landfall is related to the intensified inflow while the pressure field remains relatively unchanged. The later decrease in the generation of total kinetic energy is due to both the weakening of the wind and filling of the central pressure. The domain average dissipation of the basic experiment acts in the same sense and after 2 h after landfall is higher than the generation. The result is a decrease in kinetic energy relative to the control experiment especially after hour 120.

One may look at the radial distribution of kinetic energy and the individual terms in the total kinetic energy budget for the two distinct periods before and after landfall (Fig. 13). The total kinetic energy difference is maximum near 60 km, which coincides with the radius of maximum winds. At radii greater than 125 km, the kinetic energy is actually slightly greater after the storm is over land. This is consistent with some observations mentioned in Section 3b which indicate a broadening of the storm as it decays. The

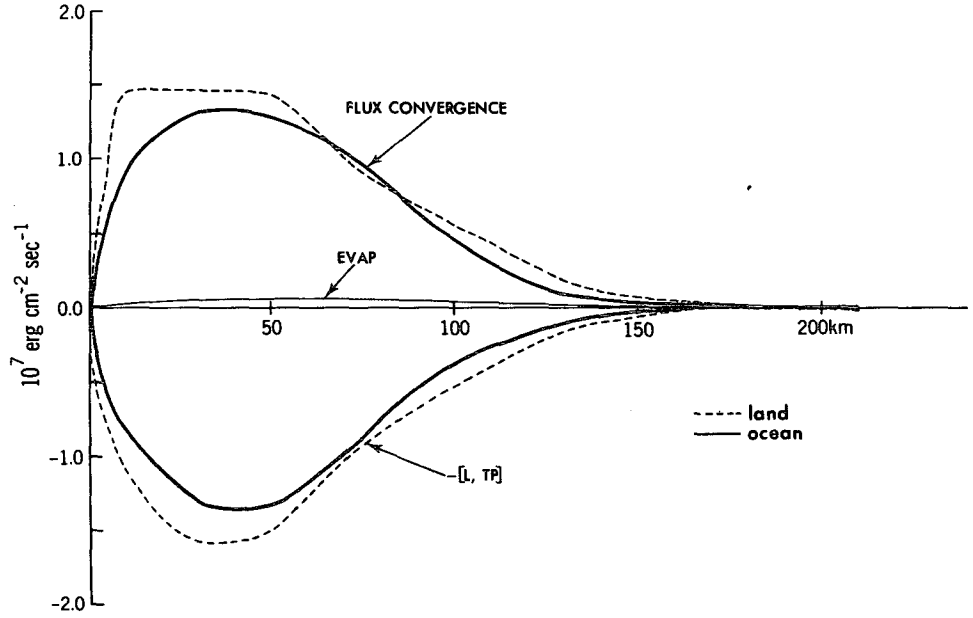

FIG. 15. Radial distribution of latent energy budget for the basic landfall experiment. Budget quantities are shown for the period over ocean (hours 103:15–107:00) and for period over land (hours 115:00–118:45). Changes due to flux convergence, evaporation and conversion to total potential energy −[L, TP] are indicated for both periods. Budget terms are vertically integrated, circularly averaged.

generation of kinetic energy has this same feature, with the generation over land typically less than that over ocean for the inner 100 km of the storm, but greater in the next 60 km. The total dissipation over land is less than that over ocean for the inner 75 km. At radii greater than 75 km, the total dissipation is greater over land than over sea. The dissipation due to vertical mixing including surface dissipation is greater over land than over ocean at all radii. In the model, however, horizontal diffusive forces are significant especially in regions of high horizontal wind shear near the storm core. For this reason the total dissipation in this inner region is greater over the sea than over rough land.

b. Total potential energy budget

Very little significant change in the temperature field occurs within seven hours of landfall over which the budget analyses were made. However, some changes in the total potential energy budget can be suggested from the comparison of the budget terms for the two periods before and after landfall. The analysis results are presented in Fig. 14. It is seen that the energy input from latent heating is greater over the land than over the ocean. This is consistent with the increased rainfall upon landfall. From 20 to 80 km, the flux convergence of internal energy over land is less than over the ocean, while the flux divergence of potential energy and pressure work is greater. These features, working to decrease the potential energy, counteract the effect of increased condensational heating, especially from 25 to 50 km. The decrease in the total potential energy contributes to the slow decay of the warm core if the surface pressure and low-level temperature changes are negligible. Near the storm center, the differences between the budget term over the ocean and over the land become large. But these computed values are probably not reliable because of interpolation problems in the analysis near the center.

c. Latent energy budget

The latent energy budget is presented in Fig. 15 for the two time periods before and after landfall. An interesting finding from this basic experiment is that, despite the reduction of moisture over land, the flux convergence of moisture is the same or even greater over land than over ocean. This, of course, is only true for the first 10 h after landfall of the model storm. The land has two opposing effects on the evolution of the storm vortex. It increases the boundary layer inflow of moisture which counteracts the depletion of surface moisture caused by lack of evaporation. In the present experiment, the increased boundary layer convergence

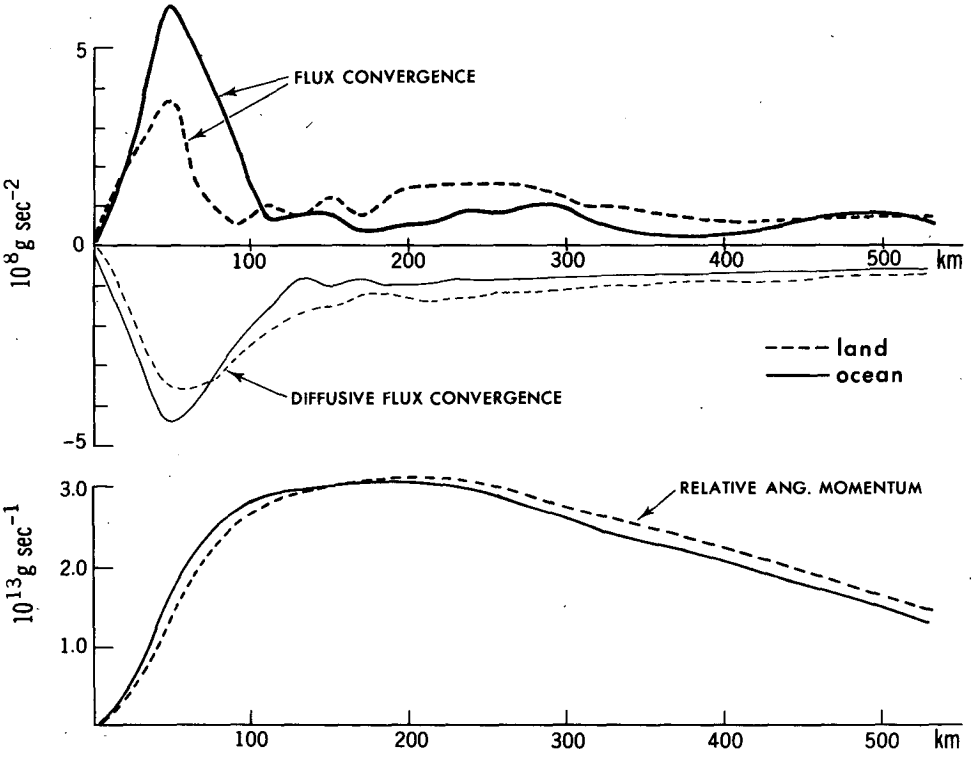

FIG. 16. Radial distribution of relative angular momentum and relative angular momentum budget for the basic landfall experiment. Budget quantities are shown for the period over ocean (hours 103:15–107:00) and for the period over land (hours 115:00–118:45). Changes due to flux convergence (thick lines) and diffusive flux convergence (thin lines) are indicated for both periods. The Coriolis turning term is too small to be graphed. Budget terms are vertically integrated, circularly averaged.

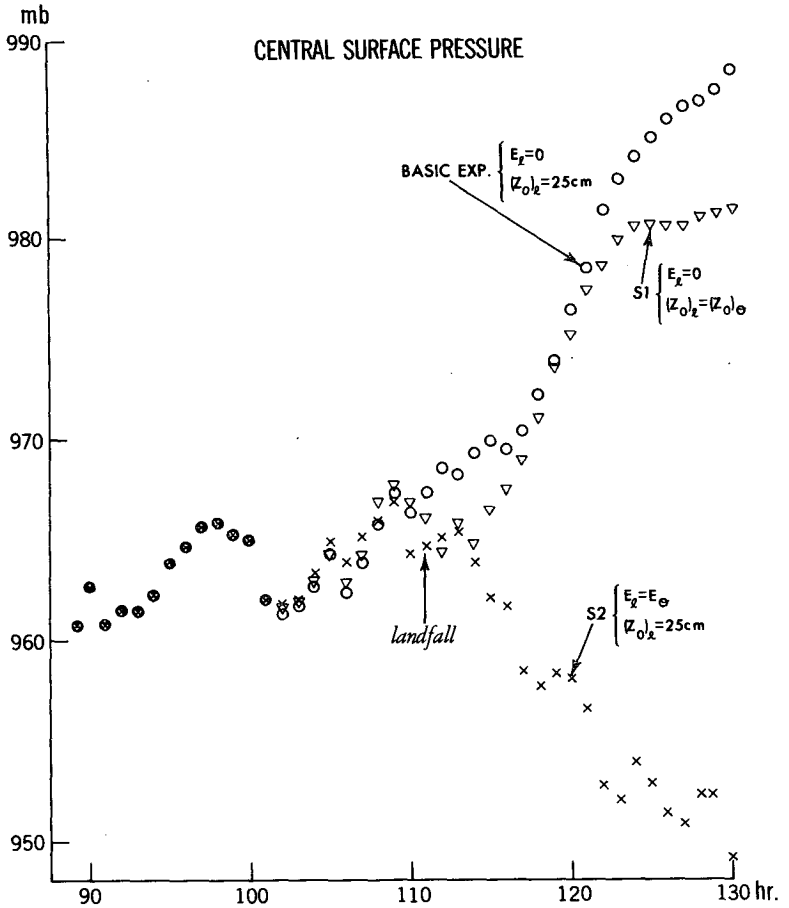

FIG. 17. Time variation of central surface pressure for the basic landfall experiment, the first supplementary experiment S1 and the second supplementary experiment S2. Landfall for all three experiments was at hour 111. E_l is the evaporation over land and $E_l = E_\theta$ denotes that the evaporation formulation was identical over land and ocean. $(Z_0)_l$ is the roughness length over land and $(Z_0)_l = (Z_0)_\theta$ denotes the formulation for roughness length was identical over land and ocean.

overcomes moisture depletion to make the moisture convergence greater. For this reason the latent heat release is greater for the first couple of hours after landfall. The reduction or elimination of evaporation has a subtle but vital effect on the moisture budget in the long run. The lack of evaporation over land eventually depletes the storm system of enough moisture to sustain sufficient release of latent heat to overcome the cooling caused by upward motion.

d. Relative angular momentum budget

The relative angular momentum and the individual terms of the relative angular momentum budget for the basic landfall experiment are shown in Fig. 16. The relative angular momentum decreases in the inner 150 km from ocean to land while it increases from ocean to land at radii greater than 150 km. As a result, for the area within 500 km, the relative angular momentum is larger over the land. The flux convergence of relative angular momentum is noticeably smaller for the inner 100 km over the land as opposed to over the ocean. At radii greater than 100 km, the flux convergence of relative angular momentum is greater over the land than ocean. This coincides with the net tendency for the relative angular momentum to increase at large radii while decreasing in the central core of the storm. The diffusive flux divergence of relative angular momentum is reduced over land for the inner 80 km of the storm, while it is greater over land for radii greater than 80 km. This is due to the decreased horizontal diffusion near the storm center over land in the model cyclone.

5. Additional experiments and analysis of decay mechanism

a. First supplementary experiment

Besides the basic experiment in which the tropical cyclone drifted over the land where the evaporation

TABLE 1. A comparison of central surface pressure, maximum surface wind, precipitation, and other domain averaged quantities among the basic landfall experiment, the two supplementary experiments, S1 and S2, and the control experiment.

	Hour	Control experiment	Basic experiment	S1	S2
Surface roughness over land		(no land)	$z_0=25$ cm	Same as over ocean	$z_0=25$ cm
Evaporation over land		(no land)	No	No	Yes
Central sfc pressure (mb)	115	965.5	969.9	966.5	962.2
	121	967.4	978.6	977.4	956.7
	130	958.3	988.5	981.6	948.8
Maximum sfc winds (m s^{-1})	115	39.6	30.6	39.7	36.3
	121	37.9	23.7	31.9	40.7
	130	48.7	18.4	27.6	43.7
Average precipitation (mm h^{-1})	115	0.046	0.047	0.030	0.059
	121	0.043	0.029	0.022	0.069
	130	0.045	0.029	0.021	0.071
Ave. KE generation (J m^{-2} s^{-1})	115	2.18	1.71	1.18	2.82
	121	1.97	1.18	0.79	3.75
	130	1.98	0.86	0.80	3.71
Ave. KE dissipation (J m^{-2} s^{-1})	115	1.52	1.68	1.39	2.11
	121	1.36	1.28	0.76	2.25
	130	1.31	0.76	0.55	2.94
Kinetic energy (10^6 J m^{-2})	115	1.27	1.25	1.26	1.33
	121	1.28	1.22	1.18	1.46
	130	1.48	1.21	1.21	1.69

was entirely suppressed and the roughness length increased to 25 cm, two other experiments were run which isolated these two factors separately.

The time variation of the central surface pressure for the two supplementary experiments as well as for the basic experiment is shown in Fig. 17. In addition, Table 1 summarizes the comparison among the basic experiment, the two supplementary experiments and the control experiment. Various quantities are shown at hour 115 (4 h after the time of landfall), hour 121 (10 h after landfall) and hour 130 (19 h after landfall). In the first supplementary experiment (S1) only the evaporation was suppressed and the roughness length formulation was assumed the same over the land as over the ocean. In this experiment the coastline asymmetries of the wind present in the basic landfall experiment did not develop, the surface winds did not decrease as rapidly and the precipitation was reduced significantly after landfall. However, the storm's filling rate for the first 10 h after landfall was about the same as the basic experiment despite the different roughness assumed. The central surface pressure of S1 was only 1.2 mb less than the basic experiment at hour 121. The total kinetic energy of the storm system differs by only an insignificant amount between the basic experiment and the first supplementary experiment. This implies that the main difference in the wind field between the basic and S1 experiments is confined to the shallow planetary boundary layer. At hour 115, the area average precipitation was 0.030 mm h^{-1} for the entire domain. The area average precipitation for the basic and control experiments were 0.047 and 0.046 mm h^{-1}, respectively. The elimination of the surface roughness change at the coastline also had a minor effect on the influx of dry air toward the storm's center. The basic surface moisture pattern is quite similar to that shown in Fig. 10 for the basic experiment except that the air is more moist with relative humidities never decreasing below 80% at landfall. This is due to both the absence of coastline subsidence to the left of the storm center and the decrease of condensation in S1. After hour 121, the experiment with smooth land decays less rapidly than the basic experiment with rough land. This may be due to the fact that the supplementary experiment's boundary layer is relatively more moist than the basic experiment's at this time and able to slow down the decay of the warm core. In the basic experiment at hour 121, the radial vertical circulation is still rather vigorous, which, in the absence of condensation, causes cooling. The precipitation and its related heating effect is decreased by this time because a significant portion of the surface moisture was condensed at landfall. Near the storm core at hour 121, the water vapor mixing ratio of the surface air ranged from 16.4 g kg^{-1} in the basic experiment to 18.1 g kg^{-1} in this supplementary experiment. At the end of the integration, hour 130, the surface pressure was 981.5 mb for S1 compared to 988.5 for the basic landfall experiment. From 2 h after landfall to the end of the integration the domain average generation and dissipation of kinetic energy for this supplementary experiment were typically less than that of both the control experiment and the basic experiment. At hour 115, the supplementary experiment's values of generation and dissipation were 1.18

and 1.39 J m^{-2} s^{-1} respectively, and the basic landfall experiment's values were 1.71 and 1.68 J m^{-2} s^{-1}, respectively.

b. Second supplementary experiment

The second supplementary experiment (S2) was designed to study the effect of an increase of roughness on a tropical cyclone vortex. The surface roughness length was increased to 25 cm where the vortex drifted over the coastline but the evaporation was not suppressed. Realistically the evaporation may be retarded over land because the land surface temperature is likely to be lower than the sea surface temperature, the ground may not be saturated and the surface winds may decrease. In this idealized experiment, the increased roughness greatly increased the efficiency of the evaporation process at the lower boundary despite any reduction of surface wind. The surface temperature was specified to be the same value as that of the ocean (302 K) and the ground was assumed saturated. From the basic experiment, we know that an increase in roughness significantly increased Ekman pumping. Together with the increase in evaporation, the moisture available for condensation in the core area was significantly increased. These effects overcame the effects of increased surface friction and adiabatic cooling so that further development of the tropical cyclone ensued soon after landfall. As shown in Fig. 17, the central pressure dropped 8 mb in the first 10 h after landfall and was 948 mb at hour 130. The precipitation rate was increased significantly compared to the basic experiment with a domain average value of 0.059 mm h^{-1} at hour 115.

The experiments performed in this study indicate that evaporation is vital for maintenance of a tropical cyclone over the land because the two experiments, basic and S1, with a cutoff of evaporation both decayed. Surface stress increase has a direct effect to drag the surface flow but this is initially compensated by another effect to increase the boundary layer convergence which supplies the core of the storm with latent heat. Evaporation supplies additional moisture locally to the surface layer and this addition becomes more vital as the storm progresses inland. As in S2, if evaporation is not depleted, a roughness increase alone will significantly increase the moisture convergence, the precipitation and the intensity of the warm core. The vital role of latent energy supply in the decay period of a tropical cyclone upon landfall was suggested by Hubert (1955) and Miller (1964) in observational studies.

c. Descriptive summary of tropical cyclone landfall and decay

From the experiments discussed above, one may develop a general picture of a tropical cyclone landfall including the principle features and decay mechanisms. Significant features apparent at landfall in the model were discussed in the previous sections of this paper and are summarized in Table 2.

The decay rates of a tropical cyclone upon landfall are dependent upon the impact of the surface roughness change and evaporation depletion on the strength of the warm core and the associated solenoidal circulation in the radial vertical plane. The model results indicate the immediate reduction of surface winds have little direct effect on this radial vertical circulation. The in-

TABLE 2. A general summary of the features and the maintenance and decay factors affecting a tropical cyclone upon landfall.

Features	Maintenance related effect	Decay related effect
Increased drag over land		Reduction of surface wind
Enhanced Ekman pumping	Increase in moisture convergence and precipitation rate Increase in latent heat release	Increased upward motion, more cooling due to adiabatic expansion Decrease in moisture content due to precipitation
Cutoff of evaporation over land		Drier surface layer, reduction of equivalent potential temperature, reduction of precipitation
Dry tongue of surface air in upper left quadrant of storm		Dry air advection to storm core
Moisture supply by onshore wind	Excessive precipitation in front right quadrant of storm	
Coastal convergence zone	Slight tendency to increase precipitation	
Coastal divergence zone		Subsidence of dry air
Zone of negative relative vorticity at the surface where winds blow onshore		

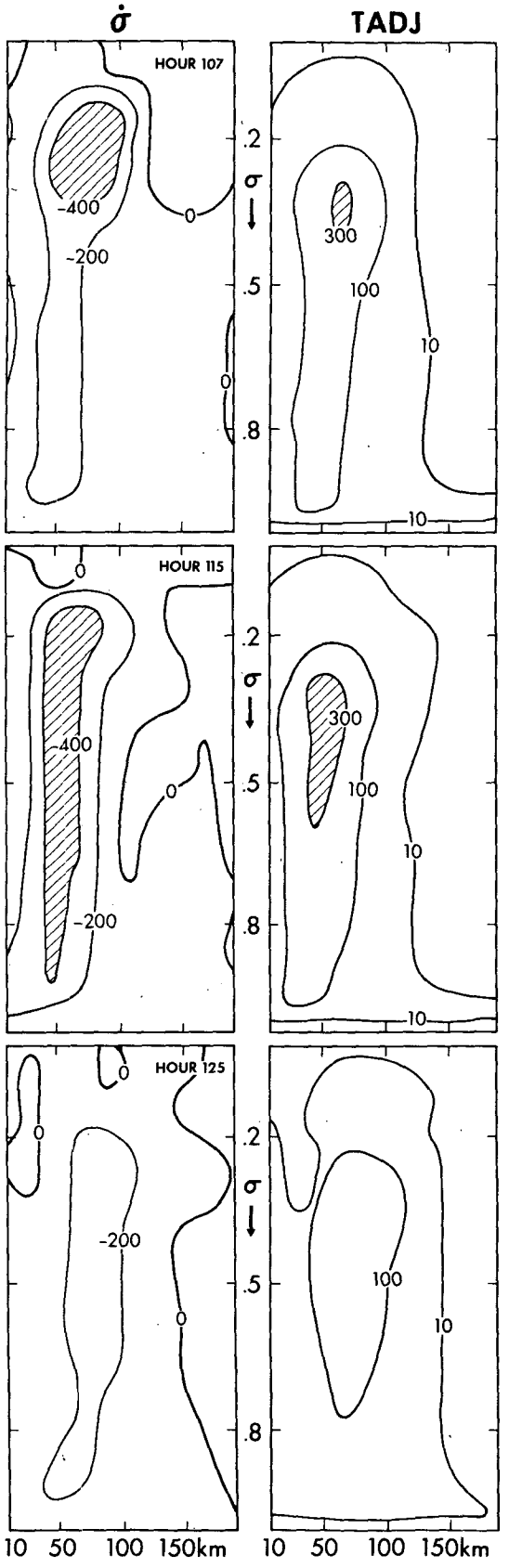

crease in roughness encountered over land reduces the tangential wind component in the boundary layer while the radial wind component may indeed increase. This enhancement of the boundary layer inflow leads to a tendency for greater convergence of moisture and consequently more precipitation and more convective heating in the warm core region. However, the increased Ekman pumping yields stronger adiabatic cooling. In addition, the depletion of evaporation over land causes the precipitation process to be less efficient, that is, the rainfall rate is smaller for the same Ekman pumping. The evolution of the warm core is determined by all of the above effects. Fig. 18 shows the radial-vertical cross sections of $\dot{\sigma}$, i.e., $d\sigma/dt$, and TADJ, the temperature adjustment due to convection four hours before and after landfall and fourteen hours after landfall for the basic experiment. Notice the increased upward motion within 50 km of the storm center between hour 107 and hour 115. The convective heating also has increased somewhat during this time, but not nearly as much as when the evaporation was not depleted. In the second supplementary experiment where the evaporation was not suppressed, the maximum convective heating at hour 115 was 6.052 mb K^1 s^{-1} at model level 4, $\sigma=0.335$, compared to a value of 4.228 mb K^1 s^{-1} for the basic landfall experiment at hour 115. The increase of the vertical-radial circulation tends to cool the warm core if heating by convection doesn't correspondingly increase (see Kurihara, 1975, pp. 32–35). The warm core will decrease slowly in magnitude at first since the convective heating is maintained by the enhancement of the surface boundary layer inflow of moisture. As the storm drifts over land, the boundary layer will become more depleted of moisture especially if the precipitation rate is maintained by increased inflow. The dehumidification of the boundary layer ultimately inhibits the precipitation process leading to further decay.

Local asymmetries may alter the decay sequence of the storm vortex. Enhanced boundary layer inflow, coastline convergence, excessive precipitation, and generation of kinetic energy in the right quadrant may tend to induce further development. However, these effects are compensated to some degree in the left quadrant of the storm where coastline divergence creates local subsidence which reduces the already low values of relative humidity. This dry air with low equivalent potential temperature is advected into the core of the storm by boundary layer inflow. It is uncertain whether these two effects exactly compensate one another, or whether the coastal asymmetries have any net effect on the decay sequence. Table 2 summarizes the critical factors affecting the maintenance and decay process of a model tropical cyclone encountering land.

FIG. 18. Radial-vertical cross sections of σ, the vertical velocity in σ coordinates, and TADJ, the mass weighted convective temperature adjustment for hour 107, hour 115 and hour 125. Units of $\dot{\sigma}$ are in 10^{-7} s^{-1} and units of TADJ are in 10^{-2} mb K s^{-1}.

6. Summary

Within a relatively simple experimental framework, simulations of landfall of tropical cyclones were successfully accomplished utilizing a version of the GFDL tropical cyclone model. The gross features of surface pressure filling and of a decay sequence upon landfall were realistically obtained. Evaporation depletion over the land was shown to be the single most important parameter in the decay sequence on landfall. Increased surface roughness tended to augment boundary layer inflow. It had little immediate impact on the storm intensity. Indeed without a cutoff of evaporation, increased surface roughness will enhance more evaporation and a more vigorous boundary layer, leading to further development. The effect of surface dissipation when encountering land is at least partially overcome by increased kinetic energy generation because of increased boundary layer inflow. Despite the gradual modification of the surface air, the increase in the boundary layer inflow maintains ample convergence of moisture for a period of time immediately after landfall. These mechanisms are supported by the analyses of the energy and angular momentum budgets before, during and after landfall.

Interesting features at landfall include coastal divergence and convergence bands which develop when winds blow on and offshore. Spiral bands exist and propagate radially outward through these stationary coastal bands. Modification of swirling moist surface air occurs on landfall and is most evident to the left of the storm's track. Surface relative humidities may decrease below 80% in the left quadrant and this decrease contributes to the weakening of the storm system. Because of the increased vigor of the boundary layer and the ample moisture supply from the ocean, the upper right quadrant of the storm is a prime location of maximum precipitation intensity during the landfall.

Finally, it should be acknowledged that the limitations of the present model experiments are still too severe to make any exact comparison of the results with real case studies. It would be advantageous to allow a steering current, surface temperature variability and topography in any future model studies.

Acknowledgments. The authors are indebted to J. Smagorinsky who has given them continued support throughout the course of the tropical cyclone project. They are also grateful to J. Hovermale, F. Lipps., S. Manabe and T. Rosati who read the original manuscript and gave useful, constructive criticism. In addition, it is a pleasure to express gratitude to J. Conner, P. Tunison and B. Williams for their assistance in the preparation of this manuscript.

REFERENCES

Eliassen, A., 1971: On the Ekman layer in a circular vortex. *J. Meteor. Soc. Japan*, **49**, 784–789.

Hubert, L., 1955: Frictional filling of hurricanes. *Bull. Amer. Meteor. Soc.*, **36**, 440–445.

Koteswaram, P., 1963: Floods and strong winds associated with tropical cyclones in the Indian Ocean. *Proc. of the Inter-regional Seminar on Tropical Cyclones*, Tokyo, Japan Meteor. Agency, Rep. No. 21, 271–277.

Kurihara, Y., 1965: On the use of implicit and iterative methods for the time integrations of the wave equation. *Mon. Wea. Rev.*, **93**, 33–46.

——, 1973: A scheme of moist convective adjustment. *Mon. Wea. Rev.*, **101**, 547–553.

——, 1975: Budget analysis of a tropical cyclone simulated in an axisymmetric numerical model. *J. Atmos. Sci.*, **32**, 25–59.

——, and R. E. Tuleya, 1974: Structure of a tropical cyclone developed in a three-dimensional numerical simulation model. *J. Atmos. Sci.*, **31**, 893–919.

Matsuno, T., 1966: Numerical integrations of primitive equations by use of a simulated backward difference method. *J. Meteor. Soc. Japan*, **44**, 76–84.

Miller, B., 1964: A study of the filling of hurricane Donna (1960) over land. *Mon. Wea. Rev.*, **92**, 389–406.

Novlan, D., and W. Gray, 1974: Hurricane-spawned tornadoes. *Mon. Wea. Rev.*, **102**, 476–488.

Ooyama, K., 1969: Numerical simulation of the life cycle of tropical cyclones. *J. Atmos. Sci.*, **26**, 3–40.

Rosenthal, S., 1971: The response of a tropical cyclone model to variations in boundary layer parameters, initial conditions, lateral boundary conditions and domain size. *Mon. Wea. Rev.*, **99**, 767–777.

Sellers, W., 1967: *Physical Climatology*. University of Chicago Press, 272 pp.

Syono, S., 1949: Approximate solution of non-linear differential equation of stationary wind in axial symmetric cyclone and anticyclone and its applications. *Geophys. Mag. Tokyo*, **20**, 39–65.

——, Y. Ogura, K. Gambo and A. Kasahara, 1951: On the negative vorticity in a typhoon. *J. Meteor. Soc. Japan*, **29**, 1–9.

Tuleya, R. E., and Y. Kurihara, 1975: The energy and angular momentum budgets of a three-dimensional tropical cyclone model. *J. Atmos. Sci.*, **32**, 287–301.

Yanai, M., 1964: Formation of tropical cyclones. *Rev. Geophys.*, **2**, 367–414.